

## Continuous Cooling Precipitation Diagrams Depending on the Composition of Aluminum-Magnesium-Silicon Alloys

Benjamin Milkereit<sup>1</sup>, Christoph Schick<sup>2</sup>, Olaf Kessler<sup>1</sup>

<sup>1</sup> University of Rostock, Faculty of Mechanical Engineering and Marine Technology,  
Chair of Materials Science, 18051 Rostock, Germany

<sup>2</sup> University of Rostock, Institute of Physics, Polymer Physics Group, 18051 Rostock, Germany

This work presents the temperature- and time dependent precipitation behavior during cooling from solution annealing of five aluminum-magnesium-silicon alloys with different compositions. The continuous cooling precipitation (CCP) diagrams of these alloys were recorded by differential scanning calorimetry (DSC). With the information out of CCP diagrams, the quenching step during the age hardening treatment could be optimized. CCP diagrams of aluminum alloys potentially will achieve the same importance like continuous cooling transformation diagrams for steels. The aluminum alloys EN AW-6060, 6063, 6005A and two compositions of 6082 were solution annealed and quenched in three different DSCs whereby the cooling rate range varies over three orders of magnitude (0.1 K/min – 375 K/min). Some alloys additionally were quenched in a dilatometer, in order to vary the cooling rate over five orders of magnitude (0.05 – 20,000 K/min). Cooling rate depending precipitate formation was analyzed by light- and scanning electron microscopy. Element composition of growing precipitates was investigated by energy dispersive x-ray spectroscopy. The crystal structures of precipitates were detected by x-ray diffraction and by electron backscatter diffraction. All alloys show a similar precipitation behavior. In an appropriate cooling rate range at least two precipitation reactions were found in different temperature ranges. It could be proven that the high temperature reaction corresponds to the precipitation of the equilibrium phase  $\beta$ -Mg<sub>2</sub>Si. The precipitation kinetic depends on the alloy content. The critical cooling rate to suppress precipitation during cooling from solution annealing rises with increasing alloy content, e.g. EN AW-6060 (0.4 mass% Si, 0.44 mass% Mg): upper critical cooling rate 50 K/min; EN AW-6082 (1.23 mass% Si, 1.05 mass% Mg): upper critical cooling rate 8000 K/min.

**Keywords:** *Continuous cooling precipitation diagrams, aluminum-magnesium-silicon alloys, DSC, Mg<sub>2</sub>Si, XRD, EBSD, microstructure, alloy composition*

### 1. Introduction

Strength of metallic material is adjusted by heat treatment in many cases. The most important heat treatment for strengthening of aluminum alloys is age hardening. Thereby the cooling rate is an important parameter. This needs to be high enough to suppress precipitation during cooling as requirement for maximal strengthening during aging. However, cooling rate should be as low as possible to avoid extensive residual stresses and distortion. The influence of cooling rate on the precipitation behavior during the quenching step of age hardening is described by continuous cooling precipitation (CCP) diagrams. CCP diagrams of aluminum alloys potentially will achieve the same importance like continuous cooling transformation diagrams for steels. During the last years a method was developed to record such diagrams in using Differential Scanning Calorimetry (DSC), detecting the exothermal precipitation heat [1-6]. A manual to use DSC for the

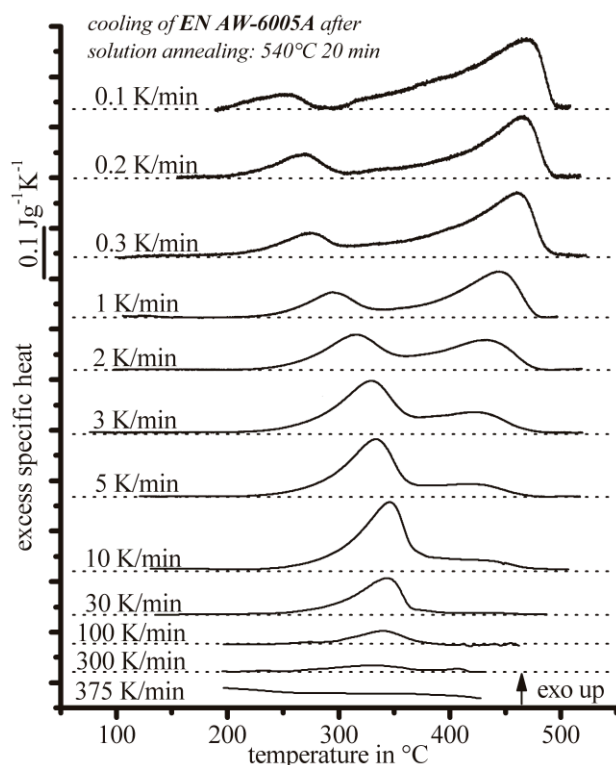


**Fig. 1:** Selected cooling curves of one composition of EN AW-6005A from three different types of DSC-devices in a cooling rate region from 0.1 K/min to 375 K/min (0.1 - 5 K/min: Setaram 121; 10 - 30 K/min: Mettler 823; 100 - 375 K/min: Perkin-Elmer Pyris 1) [4].

measurement of precipitation reactions in aluminum alloys is described and discussed in [4]. For EN AW-6005A at least two exothermal reactions have been detected during cooling, a high- and a low-temperature reaction respectively. Figure 1 displays selected DSC cooling curves as functions of temperature. The curves are arranged one below the other downwards with increasing cooling rate. The zero line of each cooling curve is shown dotted. Deviations upwards from this zero lines signify exothermal reactions.

Applying metallographic analyses by light- and scanning electron microscopy (SEM), energy dispersive X-ray spectroscopy (EDX), X-ray diffraction (XRD) and electron backscatter diffraction (EBSD) on EN AW-6005A it was shown that the high temperature reaction corresponds to the precipitation of the equilibrium phase  $\beta$ -Mg<sub>2</sub>Si [7]. Continuous cooling precipitation diagrams of three compositions of Al-Mg-Si alloys have been published in a small range of cooling rates (some 10 to some 100 K/min) [3]. By these results we can conclude that precipitation kinetic depends on the alloy content: the cooling rate to suppress precipitation rises with increasing alloy content. However, according to [4], the scope of these investigations has been insufficient in cooling rate range.

The purpose of this report is to compare the precipitation behavior during cooling and also the microstructure evolution depending on the composition of aluminum-magnesium-silicon alloys with an excess of silicon over a wide range of cooling rates.

## 2. Materials and methods

Five alloys out of the system Al-Mg-Si with an excess of Si were investigated. Mass fractions of alloying elements are given in Table 1. By comparing the results of [3], [4] and [7] we come to the conclusion that for a complete understanding of the thermal precipitation behavior during cooling

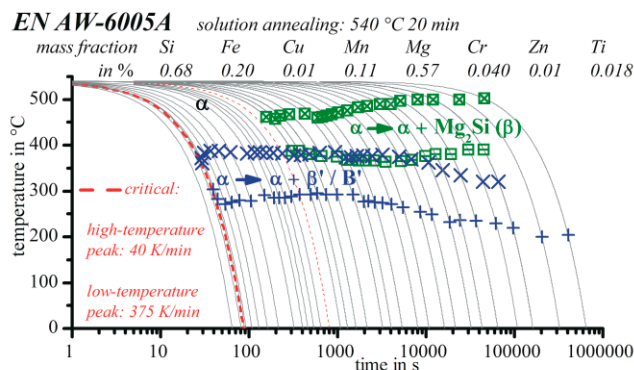


**Fig. 2:** Continuous cooling precipitation diagram of one composition of EN AW-6005A

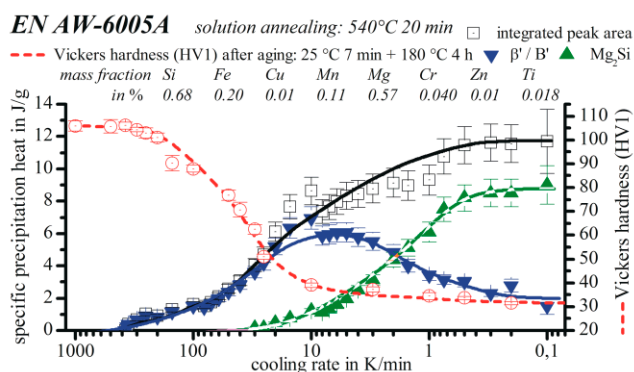


**Fig. 3:** Specific precipitation heat after cooling to room temperature and Vickers hardness (HV1) after artificial aging of one composition of EN AW-6005A as functions of cooling rate. [4, 7]

**Table 1: Mass fractions of alloying elements in investigated compositions**

mass fraction in %	Si	Fe	Cu	Mn	Mg	Cr	Zn	Ti
EN AW-6060	0.4	0.2	0.01	0.02	0.44	0.001	0.01	0.009
EN AW-6063	0.5	0.19	0.02	0.03	0.47	0.005	0.03	0.013
EN AW-6005A	0.68	0.2	0.01	0.11	0.57	0.04	0.01	0.018
EN AW-6082 <sub>low</sub>	0.73	0.22	0.05	0.48	0.61	0.003	0.009	0.02
EN AW-6082 <sub>high</sub>	1.23	0.2	0.09	0.65	1.05	0.2	0.05	0.03

from solution annealing it is important to observe all cooling rates of technical interest: from conditions close to equilibrium to complete supersaturation of solid solution.

We define a lower critical cooling rate (ICCR) for begin of supersaturation in solid solution and an upper critical cooling rate (uCCR) for complete supersaturation of solid solution).

All five compositions were investigated by DSC in the cooling rate range available (three orders of magnitude – from about 0.2 K/min to 400 K/min). The cooling rate range was enlarged by a quenching dilatometer, for microstructure analyses and hardness testing, to about five orders of magnitude (0.05 K/min – 20,000 K/min).

Hardness testing was done after artificial aging. It is known that a delay at room temperature after quenching before the artificial aging has a significant influence on the aging response in the Al-Mg-Si system [8-9]. Hence different aging procedures were selected:

- solution annealing: 540 °C, 20 min;
- aging:
  - EN AW-6063, 6005A , 6082: 25 °C, 7 min + 180 °C, 4 h;
  - EN AW-6060: 25 °C, 48 h + 180 °C, 4 h.

To compare the alloys, the precipitation behavior was investigated by DSC and additionally the microstructure was analyzed by light- and scanning electron microscopy (SEM), energy dispersive X-ray spectroscopy (EDX), X-ray diffraction (XRD), electron backscatter diffraction (EBSD) and also hardness tests at varying cooling conditions.

### 3. Results

The most important finding is that all investigated alloys have shown a similar precipitation behavior with a high- and a low-temperature precipitation reaction. There are indications for some more reactions. However, only at EN AW-6082<sub>low</sub> a middle-temperature reaction was surely identified. All alloys have a similar temperature-range of precipitation. The start temperatures of precipitation raised with increasing alloy content. In Figure 2 the first available complete CCP diagram of an aluminum alloy is presented using the example of the investigated composition of EN AW-6005A. The CCP diagram informs if to any time at any temperature a precipitation reaction will occur. No information about the intensity of possible reactions are given by the CCP diagram. This important information can be read out of diagrams which display the specific precipitation heat during cooling and the hardness after aging as functions of cooling rate (Figure 3 and 4). For the analyzed composition EN AW-6005A hardness after artificial aging showed maximum values as long as no precipitation heat could be observed during cooling, because aging started with a complete supersaturated solid solution.

Figure 4 shows a comparison of all investigated alloys (a) by their total specific precipitation heat during cooling and (b) also by their Vickers hardness (HV1) after artificial aging as functions of cooling rate. The cooling rates axes are scaled decreasing logarithmic for comparability with the time scale of CCP diagrams. The total specific heat of all investigated compositions rose with decreasing cooling rate. The hardness of all alloys decreases with decreasing cooling rate, as long as cooling was done slower than the uCCR.

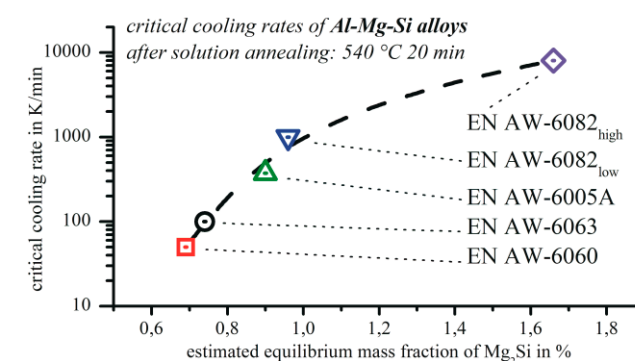
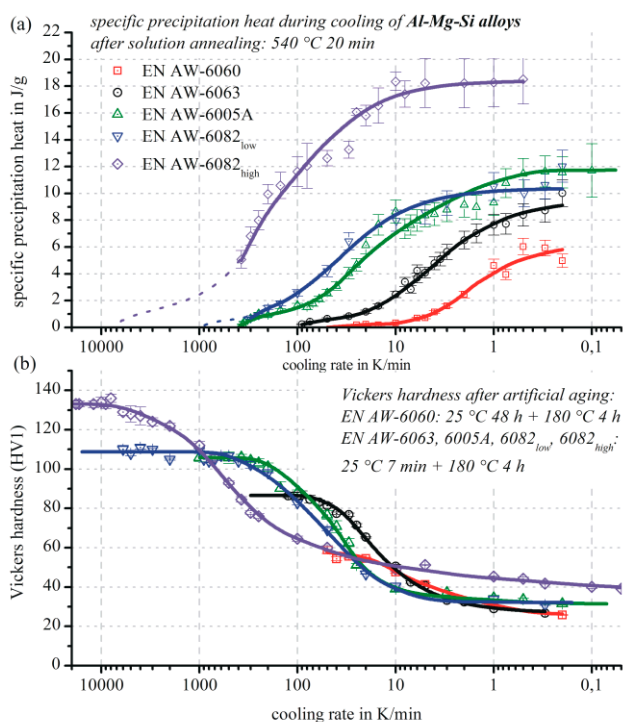


**Fig. 5: Upper critical cooling rate of Al-Mg-Si alloys depending on alloy content**

**Fig. 4: (a) total specific precipitation heat during cooling of five Al-Mg-Si alloys; (b) Vickers hardness (HV1) after artificial aging, both as functions of cooling rate**

The precipitation kinetic depended on the alloy content: upper and lower critical cooling rate increased with increasing alloy content (Figures 4 and 5). The maximum values of total released heat also increased with increasing alloy content. Generally the precipitation heat decreases with increasing cooling rate due to the suppression of diffusion processes. We have shown that the precipitation heat is directly proportional to the mass fraction and thereby also approximately to the volume fraction of precipitates [7].

For EN AW-6060, 6063 and 6005A it is clearly visible in Figure 4 that maximum hardness values were reached if just no precipitation heat could be detected. Comparing the development of Vickers hardness and precipitation heat one can conclude that the curves proceed inversely. Knowing this we could estimate the development of precipitation heat for both compositions of EN AW-6082 (extrapolation of precipitation heat fit, dotted lines in Figure 4 (a)). Hence it was also possible to estimate the uCCR of both compositions of EN AW-6082 (Figure 5).

The values of total precipitation heat were constant as long as the cooling rate was slower than a alloy specific ICCR. Such constant specific precipitation heat values at relatively low rates could be detected for three alloys (EN AW-6082<sub>high</sub>, 6082<sub>low</sub> and 6005A).

Figure 5 shows the uCCR depending on alloy content of Al-Mg-Si alloys. The cooling rate axis is scaled logarithmic. From the alloy content a mass fraction of Mg<sub>2</sub>Si at equilibrium for room temperature has been estimated. The uCCRs raised significantly with increasing alloy content. Between a Mg<sub>2</sub>Si mass fraction of about 0.7 % and 1.65 % an increase in uCCR of about two orders of magnitude was detected. Even inside the composition standard EN AW-6082 differences between low and high alloyed compositions of nearly one order of magnitude occur. Hence, it must be mentioned, that the results are only valid for the investigated chemical compositions. This applies for initial microstructures and solution annealing conditions too.

XRD analyses on samples cooled with 0.05 K/min (close to equilibrium conditions) verify the presence of the fcc lattice of  $\beta$ -Mg<sub>2</sub>Si ( $a = 0.635$  nm) for all alloys. For EN AW-6005A this was proven by EBSD analyses [7]. For EN AW-6063, 6005A and 6082<sub>low</sub> it was possible to show that  $\beta$ -Mg<sub>2</sub>Si forms at the high temperature reaction by interrupted cooling and metallographic analyses (details for EN AW-6005A in [7]). If  $\beta$ -Mg<sub>2</sub>Si is precipitated inside of aluminum grains it will form plates perpendicular to each other, possibly on {100} planes of the aluminum solid solution [7]. There are strong indications that  $\beta$ -Mg<sub>2</sub>Si particles nucleate at primary precipitates (consisting mainly of Fe,

Si, Mn). In any analyzed  $\beta$ -Mg<sub>2</sub>Si particle we found primary precipitates, even if the  $\beta$ -Mg<sub>2</sub>Si particle was located on a grain boundary. For EN AW-6005A first TEM results indicate that the low-temperature reaction corresponds to the precipitation of  $\beta'$ /B' phase.

#### 4. Discussion

The precipitation behavior of different Al-Mg-Si alloys, with an excess of Si, during cooling from solution annealing is similar (Figure 4). Particularly there are at least two main exothermal reactions and similar precipitation temperature ranges for each alloy (see examples in Figure 1 and Figure 2). The start temperature of the Mg<sub>2</sub>Si precipitation and the specific precipitation heat increased significantly with increasing alloy content. The increase of start temperature is expected from the quasi-binary phase diagram Al-Mg<sub>2</sub>Si. The findings of this work confirm the results of [3], where mainly the high-temperature peak was detected because of the small cooling rate range. Additionally the results of this work demonstrate that it is essential to follow the whole range of cooling rates of technical interest: from conditions close to equilibrium up to the complete suppression of precipitation for the CCP diagram.

Some DSC-curves show overlapping peaks (Figure 1). One possibility to separate overlapping peaks is presented in [4] by fitting two gauss curves. Although this fits not perfectly, it is a possible way to draw conclusions about the volume fraction of the precipitated phases from the DSC-signal [4; 7]. According to our understanding no sharp separation of single reactions is possible. Rather it seems that the precipitation process during cooling can be divided in at least two main overlapping sections: the precipitation of  $\beta$ -Mg<sub>2</sub>Si and the precipitation of the phases  $\beta'$ /B'. Thereby some more reactions could be involved in detail. For example during the forming of  $\beta$ -Mg<sub>2</sub>Si at least two different nucleation mechanisms take place: nucleation on grain boundaries and nucleation inside of aluminum solid solution grains, both probably starting on primary precipitates. Very likely these different nucleation mechanisms take place concurrently, competing about the alloying element atoms with different nucleation energies and diffusion ways.

In contrast to steels the critical cooling rates of Al-Mg-Si alloys raise with increasing alloy content (Figure 5). This finding confirms the results of earlier reports [2-3; 5-6] and can be explained by the higher supersaturation of the higher alloyed materials.

For three alloys (EN AW-6060, 6063, 6005A) hardness after aging proceeds inversely to the precipitation heat during cooling. Therefore it can be assumed that the extrapolated uCCR of both compositions of EN AW-6082 are accurate, at least in their order of magnitude. Compared to EN AW-6060, 6063, 6005A and 6082<sub>low</sub>, the investigated composition EN AW-6082<sub>high</sub> had a significantly lower grain size. The uCCR of this composition is about one order of magnitude higher than the uCCR of the low alloyed composition of EN AW-6082. This may be explained by the higher alloy content as well as by the smaller grain size (more nucleation sites).

During cooling with rates slower than alloy specific ICCR all alloying element atoms above equilibrium solubility can precipitate from the solid solution. Thus precipitation heat and also the mass (and volume) fraction of precipitates are constant. At significantly lower rates secondary precipitates become larger at constant volume fraction [7]. For the low alloyed compositions EN AW-6060 and 6063 the ICCR could not be detected, because even the slowest cooling rates in the used DSCs were too fast. For future work a new CALVET DSC (Setaram C 600) device is available which extends the range of possible cooling rates down to 0.01 K/min.

Further, higher cooling rates than some hundred K/min should be investigated. This would enable us to follow the precipitation behavior of high alloyed compositions by DSC up to their uCCR. The fast scanning chip calorimeter used in [10] seems to be most suitable for this aim. As the DSC-curves of all investigated alloys are similar we conclude that the metallographic findings of EN AW-6005A, are transferrable to the other investigated alloys. For the high temperature reaction, the precipitation of  $\beta$ -Mg<sub>2</sub>Si, this is confirmed by metallographic analyses, EDX and XRD results.

## 5. Summary

The precipitation behavior of five Al-Mg-Si alloys with an excess of Si during cooling from solution annealing was investigated by the means of DSC, metallographic analyses, SEM, XRD, EBSD and also hardness tests in a wide range of cooling rates (0.05 K/min – 20,000 K/min). These alloys have a similar precipitation behavior consisting of a high temperature precipitation of  $\beta$ -Mg<sub>2</sub>Si and a low temperature precipitation of, according to first TEM results, presumably  $\beta'$ /B'. For all five alloys the precipitation reactions occurred in similar temperature ranges. The start temperature of  $\beta$ -Mg<sub>2</sub>Si precipitation increased with increasing alloy content like it is to expect from the quasi-binary phase diagram Al-Mg<sub>2</sub>Si. Also the total specific precipitation heat increased with increasing alloy content.

The precipitation kinetic depended on the alloy content. Both lower and upper critical cooling rate (ICCR – begin of supersaturation of solid solution / uCCR – complete supersaturation of solid solution) raised with increasing alloy content. This can be explained by the higher supersaturation of the higher alloyed materials.

## Acknowledgement

The authors gratefully acknowledge funding of the quenching and deformation dilatometer by Deutsche Forschungsgemeinschaft and the State Mecklenburg-Vorpommern (DFG INST 264/40-1).

## References

- [1] T. Herding, O. Kessler, F. Hoffmann, P. Mayr, An approach for Continuous Cooling Transformation (CCT) diagrams of aluminium alloys, in: P.J. Gregson, H.S. J., (Eds.), 8 th International Conference on Aluminium Alloys Their Physical and Mechanical Properties, Trans Tech Publications Ltd, Cambridge, UK, 2002, pp. 869-874.
- [2] O. Kessler, R. von Bargaen, F. Hoffmann, H.W. Zoch, Continuous cooling transformation (CCT) diagram of aluminum alloy Al-4.5Zn-1Mg, in: W.J. Poole, M.A. Wells, D.J. Lloyd, (Eds.), 10 th International Conference on Aluminium Alloys 2006, Pts 1 and 2, Trans Tech Publications, 2006, pp. 1467-1472.
- [3] B. Milkereit, O. Kessler, C. Schick, Continuous Cooling Precipitation Diagrams of Aluminium-Magnesium-Silicon Alloys, in: J. Hirsch, B. Skrotzki, G. Gottstein, (Eds.), 11th International Conference on Aluminium Alloys, Deutsche Gesellschaft für Materialkunde e.V.; WILEY-VCH Weinheim, Aachen, Germany, 2008, pp. 1232-1237.
- [4] B. Milkereit, O. Kessler, C. Schick, Recording of continuous cooling precipitation diagrams of aluminium alloys. *Thermochimica Acta* 492 (2009) 73-78.
- [5] A. Deschamps, G. Texier, S. Ringeval, L. Delfaut-Durut, Influence of cooling rate on the precipitation microstructure in a medium strength Al-Zn-Mg alloy. *Materials Science and Engineering a-Structural Materials Properties Microstructure and Processing* 501 (2009) 133-139.
- [6] R. von Bargaen, O. Kessler, H.W. Zoch, Kontinuierliche Zeit- Temperatur- Ausscheidungsdiagramme der Aluminiumlegierungen 7020 und 7050. *HTM Zeitschrift für Werkstoffe, Wärmebehandlung, Fertigung* 62 (2007).
- [7] B. Milkereit, L. Jonas, C. Schick, O. Kessler, Das kontinuierliche Zeit- Temperatur- Ausscheidungs-Diagramm einer Aluminiumlegierung EN AW-6005A. *HTM Journal of Heat Treatment and Materials* 65 (2010) in press.
- [8] H. Zoller, A. Ried, Metallurgical aspects in development of AlMgSi alloys with a low sensitivity to quenching. *Z. Metallk.* 62 (1971) 354-358.
- [9] H. Zoller, A. Ried, Metallkundliche Grundlagen der leicht preßbaren AlMgSi-Legierungen. *Aluminium* 41 (1965) 626-629.
- [10] Y.L. Gao, E. Zhuravlev, C.D. Zou, B. Yang, Q.J. Zhai, C. Schick, Calorimetric measurements of undercooling in single micron sized SnAgCu particles in a wide range of cooling rates. *Thermochimica Acta* 482 (2008) 1 - 7